

An order–disorder twin crystal of L-2-haloacid dehalogenase from *Sulfolobus tokodaii*

Carrie A. Rye,^a Michail N. Isupov,^a Andrey A. Lebedev^b and Jennifer A. Littlechild^{a*}

^aHenry Wellcome Building for Biocatalysis, School of Biosciences, University of Exeter, Stocker Road, Exeter EX4 4QD, England, and ^bStructural Biology Laboratory, Department of Chemistry, University of York, Heslington, York YO10 5YW, England

Correspondence e-mail:
j.a.littlechild@exeter.ac.uk

Received 17 January 2007
Accepted 29 May 2007

The L-2-haloacid dehalogenase enzymes catalyse the hydrolytic cleavage of a halogen from the C2 position of short-chain haloacids. The recombinant dehalogenase from the thermophilic archaeon *Sulfolobus tokodaii* has been cloned, overexpressed and purified to homogeneity. The 24 kDa enzyme was crystallized using the microbatch method in the monoclinic space group *C*2, with unit-cell parameters $a = 127.6$, $b = 58.1$, $c = 51.2$ Å, $\beta = 97.2^\circ$. Data were collected to 1.9 Å resolution using synchrotron radiation and the structure was solved by molecular replacement. Analysis of the data and the preliminary refined model showed that the crystal was an order–disorder twin by reticular merohedry with a twin index of 10. It was possible to detwin the experimental data utilizing the symmetry of the molecular layers from which the crystal is built.

1. Introduction

The 2-haloacid dehalogenases (EC 3.8.1.2; halohydrolyses) catalyse the hydrolytic dehalogenation of 2-haloalkanoic acids to produce 2-hydroxyalkanoic acids. They are only active on compounds in which the halogen is attached at the C2 position. The 2-haloacid dehalogenases have important implications in the biodegradation of toxic halogenated compounds from the environment. Many of these compounds are produced synthetically for use as herbicides and growth regulators (Allpress & Gowland, 1998) and over 60% of herbicides contain at least one Cl atom (Slater, 1982). Owing to the importance of removing halogenated compounds from the environment, there has been much interest in dehalogenase enzymes.

Based on substrate specificity, three different types of haloacid dehalogenase have been identified. The three types are given the prefixes DL, D and L. DL-haloacid dehalogenases work equally well on both enantiomers of the haloacid, with either retention or inversion of the stereochemistry at the C2 atom position. D- and L-2-haloacid dehalogenases are specific to only one enantiomer and cause an inversion in the C2 configuration of the hydroxyalkanoic acid produced (Slater *et al.*, 1997). At a primary structure level, 2-haloacid dehalogenases can be divided into two groups (I and II) which do not share any sequence similarity, which suggests that they are unrelated in evolution (Hill *et al.*, 1999). Group I contains the D- and DL-haloacid dehalogenases and group II contains the L-haloacid dehalogenases.

Sequence analysis and mutagenesis studies have indicated that several dehalogenases are homologous to enzymes that carry out transformations on nonhalogenated substrates (Koonin & Tatusov, 1994). L-2-Haloacid dehalogenases belong to a large superfamily, the haloacid dehalogenase (HAD, Pfam PF00702) superfamily. All members of this family have a completely conserved aspartic acid residue. Alongside haloacid dehalogenases, this family also includes some ATPases, epoxide hydrolases and a number of different phosphatases.

X-ray structures are available for two mesophilic L-2-haloacid dehalogenases: L-DEX YL from *Pseudomonas* sp. YL (Hisano *et al.*, 1996) and Dh1B from *Xanthobacter autotrophicus* GJ10 (Franken *et al.*, 1991). Both of these enzymes are homodimers, with each subunit having a core domain of a Rossmann-fold-like six-stranded parallel

Table 1

Data-processing statistics for the synchrotron data set.

Values in parentheses are for the outer resolution shell.

| | |
|---------------------------------|--|
| Space group | C2 |
| Unit-cell parameters (Å, °) | $a = 127.6, b = 58.1, c = 51.2,$ $\alpha = 90.0, \beta = 97.2, \gamma = 90.0$ |
| Wavelength (Å) | 1.729 |
| Data-collection temperature (K) | 100 |
| Resolution range (Å) | 25–1.9 (1.93–1.90) |
| No. of measured reflections | 99871 |
| No. of unique reflections | 28692 |
| Completeness (%) | 97.6 (75.0) |
| $I > 3\sigma(I)$ (%) | 90.0 (51.0) |
| $I/\sigma(I)$ | 16 (5.7) |
| R_{sym}^{\dagger} (%) | 9.6 (16.1) |

$\dagger R_{\text{sym}} = \sum_h \sum_l |I(h) - I_l(h)| / \sum_h \sum_l I(h)$, where $I(h)$ is the intensity of reflection h , \sum_h is the sum over all reflections and \sum_l is the sum over J measurements of the reflection.

β -sheets flanked by five α -helices and a four-helix-bundle subdomain. The monomeric structure of a putative haloacid dehalogenase (PH0459) from the thermophilic archaeon *Pyrococcus horikoshii* OT3 has also recently been reported (Arai *et al.*, 2006).

The dehalogenase enzyme described in this paper is from *Sulfolobus tokodaii* strain 7, which was isolated from Beppu hot springs in Kyushu, Japan in 1983. This organism is a member of the Crenarchaeota, which traditionally comprise a close-knit group of several genera united by an extremely thermophilic sulfur-metabolizing phenotype (Woese *et al.*, 1990). *S. tokodaii* is able to convert hydrogen sulfide to sulfate and grows optimally at 353 K in an aerobic acidic sulfur-rich environment. The genome has been sequenced using the whole-genome shotgun method (Kawarabayasi *et al.*, 2001). The putative L-2-haloacid dehalogenase sequence has been identified from the genome sequence and has 31% sequence identity to L-DEX YL, 28% to DhIB and 29% to PH0459. The *Sulfolobus* dehalogenase has been cloned, overexpressed, purified and shown to have haloacid dehalogenase activity.

2. Materials and methods

2.1. Protein cloning, expression and purification

The gene coding for the L-2-haloacid dehalogenase was cloned into the pET28a expression vector, which incorporates an N-terminal six-His tag, and was overexpressed in *Escherichia coli* BL21. The *E. coli* cells containing the expressed protein were resuspended in 10% (w/v) buffer A (20 mM Tris–HCl pH 6.5) and disrupted by sonication on ice. The insoluble cell debris was removed by centrifugation at 12 000g and the supernatant was applied onto a 30 ml nickel affinity chromatography column (Ni Sepharose High Performance, GE Healthcare) pre-equilibrated with buffer A. Unbound protein was removed with buffer A and the His-tagged protein was eluted with a five column-volume gradient to 100% buffer B (20 mM Tris–HCl, 1 M imidazole pH 6.5). The dehalogenase-containing fractions were pooled and concentrated to 2 ml and applied onto a 120 ml gel-filtration chromatography column (Superdex 200 Hiload 16/60, Pharmacia) pre-equilibrated with buffer C (50 mM $\text{KH}_2\text{PO}_4/\text{K}_2\text{HPO}_4$, 100 mM NaCl pH 6.5). The protein was eluted over one column volume of buffer C. All purification steps were carried out at 277 K. The purity of the protein was analysed by SDS–PAGE (Laemmli, 1970) and the concentration of the pure protein was calculated by measuring the absorbance at 280 nm using the method of Warburg & Christian (1941). The extinction coefficient was calculated from the protein sequence (Gill & von Hippel, 1989) using the ExPasy database (Bairoch & Apweiler, 2000) to be

32 430 $M^{-1} \text{cm}^{-1}$. The concentration of dehalogenase corresponding to one absorbance unit is 1.4 mg ml^{-1} .

2.2. Enzyme activity

The L-2-haloacid dehalogenase activity was detected by a modified colorimetric assay based on the method of Holloway *et al.* (1998). The reaction mixture contained 1 mM HEPES, 15 mM sodium sulfate, 1 mM EDTA, 10 mM 2-chloropropionic acid or 2-bromopropionic acid and 2 μl phenol red solution. The assay mixture was incubated at 323 K for 5 min before the addition of 20 μl of the dehalogenase enzyme. The activity was detected by the colour change from pink to yellow, which could be measured by the decrease in absorbance at 540 nm.

2.3. Crystallization

Crystallization was carried out by the microbatch method using an Oryx 8 robot (Douglas Instruments) at 290 K. Prior to crystallization, the protein was concentrated to 10 mg ml^{-1} using a 10 kDa molecular-weight cutoff Vivaspinn centrifugal concentrator (Vivascience Ltd). A 1:1 ratio of protein to precipitant was used. Initial crystallization trials were performed using pHClear screens (Nextal Biotech). Two potential crystallization conditions were identified: (i) 100 mM HEPES, 20% (w/v) PEG 6000 pH 7.0 and (ii) 150 mM MES, 16% (w/v) PEG 6000 pH 5.5. The crystallization conditions were optimized by variation of the pH, buffer concentration and PEG concentration.

2.4. Crystallographic data collection

Data were collected at 100 K at Daresbury SRS station 10.1 (Cianci *et al.*, 2005) using a MAR 225 CCD detector from a single crystal grown under condition (i) above. The cryogenic liquor contained 100 mM HEPES, 10% (w/v) PEG 6000, 30% (w/v) PEG 400 pH 7.0. Data were processed using the programs DENZO and SCALEPACK (Otwinowski & Minor, 1997). The CCP4 package of crystallographic programs (Collaborative Computational Project, Number 4, 1994) was used for data reduction, molecular replacement and refinement.

3. Results and discussion

The purified recombinant L-2-haloacid dehalogenase migrated on SDS–PAGE as a single band of 24 kDa. Gel-filtration analysis estimated the size of the protein to be 50 kDa, suggesting that the enzyme exists as a homodimer. The colorimetric enzyme assay detected dehalogenase activity towards both of the substrates tested, 2-chloropropionic acid and 2-bromopropionic acid.

Monoclinic crystals (condition i) grew in three weeks to dimensions of $0.3 \times 0.2 \times 0.1$ mm. The crystals diffracted to beyond 1.9 Å using synchrotron radiation. They belong to space group C2, with unit-cell parameters $a = 127.6, b = 58.1, c = 51.2$ Å, $\beta = 97.2^\circ$. A summary of the X-ray data is presented in Table 1. The solvent content of the crystals, which contain two subunits in the asymmetric unit, has been estimated at 37%; $V_M = 1.96$ Å³ Da⁻¹ (Matthews, 1968).

Molecular replacement was carried out with the program MOLREP (Vagin & Teplyakov, 1997) using the haloacid dehalogenase from *X. autotrophicus* (PDB code 1qq5), which has 28% sequence identity to the *S. tokodaii* dehalogenase. The molecular-replacement solution could only be found when the search model was trimmed according to its sequence alignment to the target protein.

This was carried out using the FILE_S option of *MOLREP* (Vagin & Teplyakov, 1997). The structure was refined using *REFMAC* 5.2 (Murshudov *et al.*, 1997) and the model was rebuilt using the program *Coot* (Emsley & Cowtan, 2004). Initial refinement gave $R = 0.42$ and $R_{\text{free}} = 0.48$. After several cycles of manual model rebuilding/refinement, the model was subjected to the *ARP/wARP* protocol (Perrakis *et al.*, 1999). The resulting model was refined to a crystallographic R factor of 0.21 and an R_{free} of 0.27 with good stereochemical parameters. These appear to be high, as all main-chain atoms of the model are clearly defined in electron density. However, the solvent structure appeared to be poorly defined and addition of solvent molecules failed to significantly lower the R factors. Inspection of the native Patterson synthesis revealed a number of strong non-origin peaks on the u axis (Fig. 1*a*). The highest of them has a height of ~ 0.2 of the origin peak. At the same time, there is no translational NCS in the structure and therefore no such peaks are present in the Patterson map calculated from the model.

Analysis of molecular packing showed that the crystal structure under consideration is a particular case of an order–disorder structure (OD structure; Dornberger-Schiff, 1956; Nespolo *et al.*, 2004). It is arranged as a stack of layers which are parallel to the crystallographic plane (0 0 1). The layers are related by translations; the Δ -symmetry (the diperiodic symmetry of a layer) is $C22(2)$ (Fig. 1*b*). As

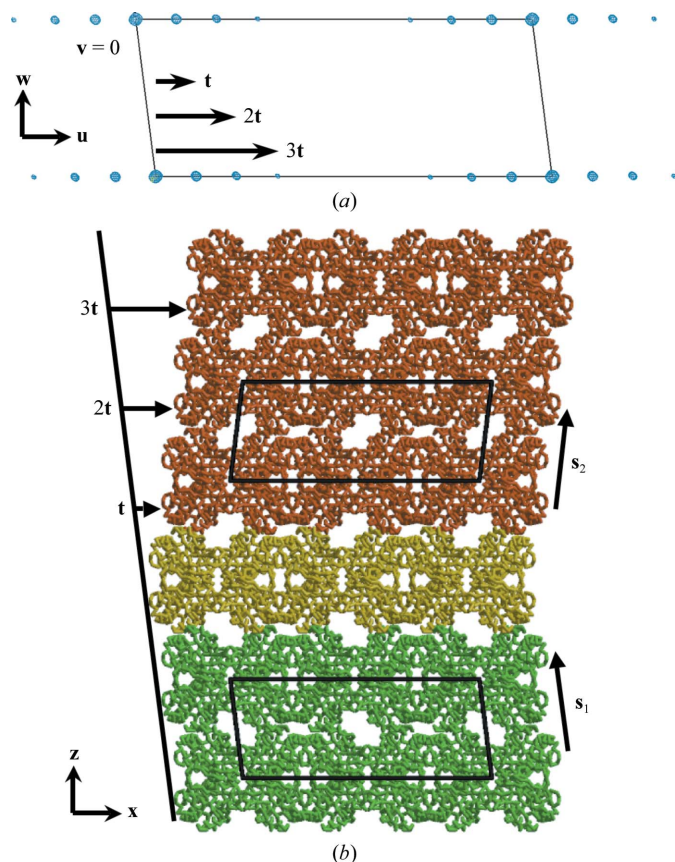


Figure 1
 (a) A section $v = 0$ of the native Patterson synthesis contoured at 4.5σ (blue). Vectors t , $2t$ and $3t$ define the positions of non-origin peaks. This figure was prepared using *Coot* (Emsley & Cowtan, 2004). (b) Possible organization of a crystal fragment including two consecutive crystal domains with local $C2$ symmetry in which layers are related by stacking vectors s_1 (green) and s_2 (orange). The intermediate layer (yellow) can be assigned to any of the two connected crystal domains. Vectors t , $2t$ and $3t$ define the offsets of three consecutive layers from their positions in a fully symmetric structure with $C2$ space-group symmetry. This figure was prepared using *BOBSRIPT* (Esnouf, 1999).

a consequence of this layer arrangement, the crystal has the potential for formation of (polysynthetic) OD twins and disordered OD structures (Dornberger-Schiff & Dunitz, 1965). A switch from stacking vector $s_1 = (-6.42, 0, 50.8)$ Å to $s_2 = (6.42, 0, 50.8)$ Å within one crystal will form a twinning interface separating two internally identical individuals (Fig. 1*b*). Layers from different individuals are related by translations, which are in agreement with the observed non-origin peaks in the Patterson map.

Some of the diffraction images clearly reveal two alternative lattices, which can be indexed with the same cell and space group (Fig. 2). Analysis of the unit-cell parameters suggests that we are dealing with a twin by reticular merohedry with twinning index 10, which is higher than Mallard’s empirical limit of six (Le Page, 2002). The estimate of the obliquity depends on the data-processing parameters and varies from 0.07 to 0.15° . According to Mallard’s law (Le Page, 2002), the twin plane must be exactly aligned with a crystallographic plane with small indices. The unit-cell parameters suggest that the twin plane is aligned with the plane (0 0 1); the twinning twofold axis is therefore parallel to c^* and another twinning twofold axis along a is generated by the crystal symmetry. The

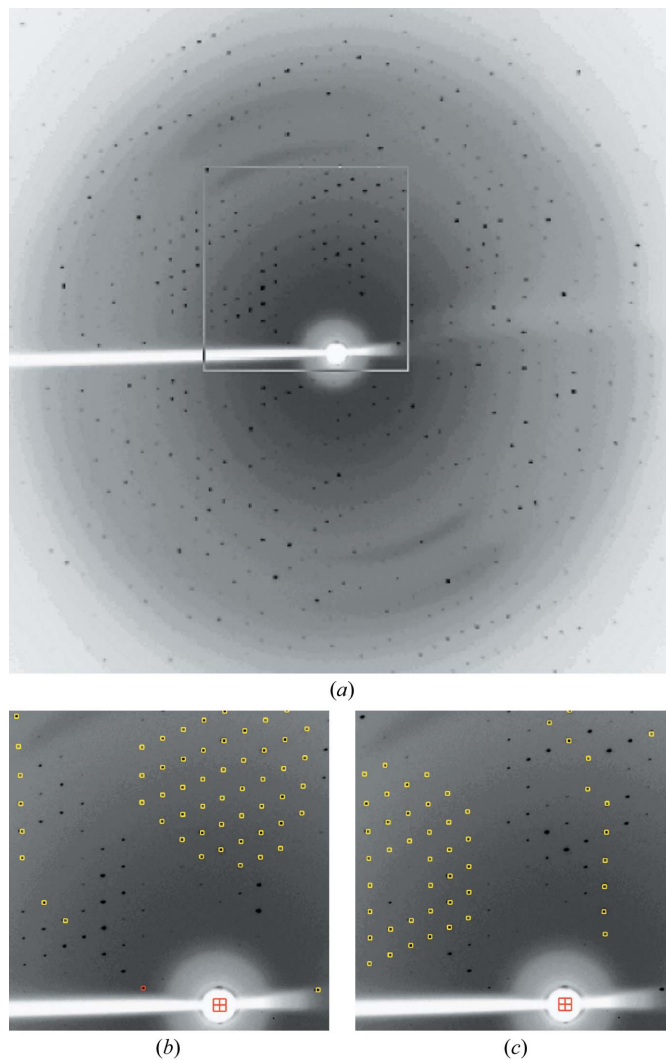


Figure 2
 Image showing the alternative lattices. (a) The whole image with the enlarged area shown by a white box. (b, c) Enlarged images with the predictions corresponding to alternative lattices. This figure was prepared using *DENZO* (Otwinowski & Minor, 1997).

perpendicular plane (1 2 0) seems to be an unlikely candidate for the twin plane because of its large second index. This is in agreement with the crystal packing, which strongly suggests that the twinning interface is parallel to the plane (0 0 1) (Fig. 1*b*). The corresponding geometry of the reciprocal space is shown in Fig. 3(*a*). Under the assumption of identical three-dimensional profiles of reflection (disregarding the geometry of data collection), the overlap q is a periodic function of index h and does not depend on indices k and l (Fig. 3*b*). Owing to the non-zero obliquity, reflections with $h = 10n$ do not overlap exactly. On the other hand, reflections with indices h close to $10n$ partially overlap owing to the non-zero size of the reflections and the small angle between a_1^* and a_2^* (Fig. 3*b*). Contributions from the alternative lattice affect the intensities of the reflections with h close to $10n$ and cause modulation of the intensities (Fig. 4*b*), which results in non-origin peaks in the Patterson map (Figs. 1*a* and 4*d*). The effect of twinning by reticular merohedry on the intensities can be modelled similarly to the case of twinning by merohedry. In our particular case, where overlapping reflections have the same index h and the overlap does not depend on k and l , the equations below can be used, where $I_{T1} = I_T(h, k_1, l_1)$ and $I_{T2} = I_T(h, k_2, l_2)$ are the measured (twinned) intensities and $I_1 = I(h, k_1, l_1)$ and $I_2 = I(h, k_2, l_2)$ are the detwinned intensities of two reflections which overlap when one of them is transformed by the twinning operator (*i.e.* belongs to the alternative lattice),

$$\begin{cases} I_{T1} = (1 - \alpha)I_1 + \alpha q(h)I_2 \\ I_{T2} = (1 - \alpha)I_2 + \alpha q(h)I_1 \end{cases} \quad (1)$$

The difference from the merohedral case is that the contribution from the alternative lattice depends on both the twinning fraction α and the overlap $q(h)$.

Our twinned crystal appears to be a polysynthetic twin with many twinning interfaces, as suggested by the lack of well defined edges.

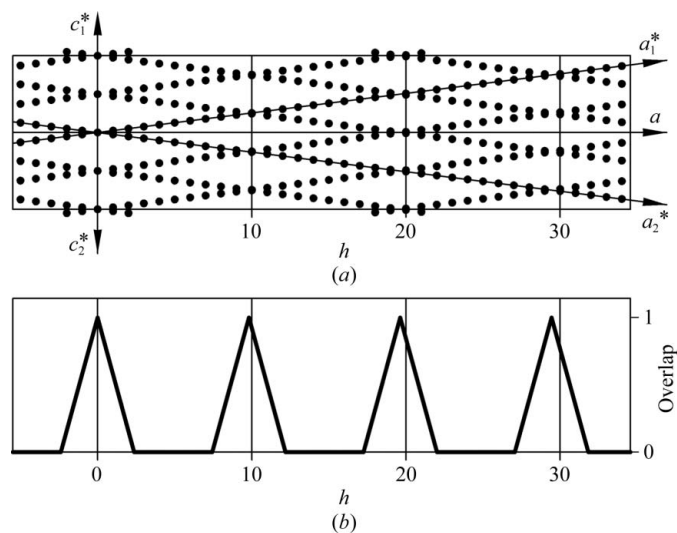


Figure 3

Arrangement of spots in reciprocal space. (*a*) A section $k = \text{constant}$ of reciprocal space. The series of close spots parallel to axes a_1^* and a_2^* belong to two alternative lattices corresponding to two different orientations of individual crystals forming a polysynthetic OD twin by reticular merohedry with twin index 10 and with obliquity 0.13° . Owing to systematic absences in C_2 , reflections with even and odd h will only appear in the real diffraction pattern in sections with even and odd k , respectively. The axes of the two equivalent twinning operators coincide with the axes c^* and a . The overlap between reflections from alternative lattices occurs only if the two reflections have the same index h and $h \approx 10n$. Because of non-zero obliquity, spots with $h = 10n$ do not overlap exactly except for $h = 0$. (*b*) If the reflections have the same size, the overlap is a periodical function of h and does not depend on k and l .

Therefore, its individuals appear to be too small to cut a single crystal out of this twin for data collection. Deconvolution of partially overlapped reflections during data processing is not yet possible with standard software for protein crystallography. Therefore, to improve our data we undertook a detwining procedure, taking into account the non-uniform overlap of the reflections from the two lattices. In principle, this can be performed using the system of equations (1).

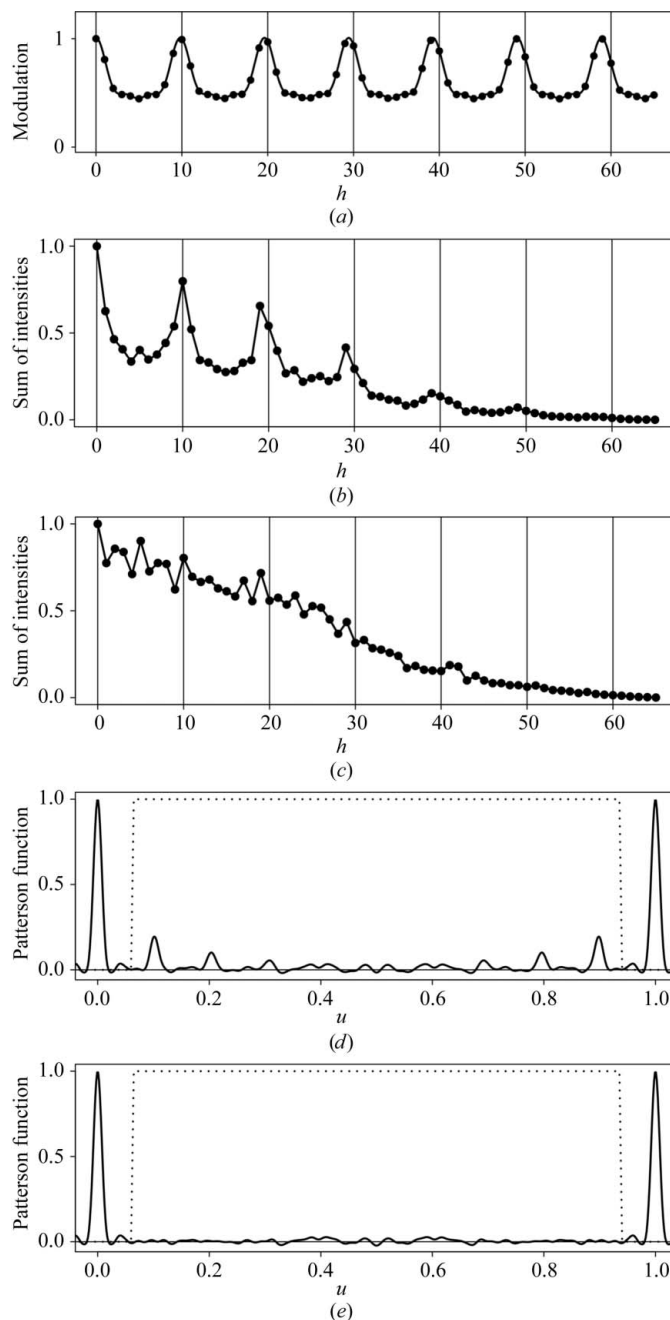


Figure 4

Demodulation of the data. (*a*) Periodic modulation function (4) with three harmonics and optimized parameters, (*b*) the sum of the measured intensities and (*c*) the sum of the demodulated intensities with given h divided by their values at $h = 0$. (*d*) The Patterson functions calculated using measured and (*e*) demodulated intensities on the line $v = w = 0$ divided by their values at $u = 0$. Relations between the plotted functions are as follows. The discrete function shown by points in (*a*) is the ratio of the discrete functions in (*b*) and (*c*). The latter two are Fourier series of the Patterson functions in (*d*) and (*e*), respectively. Optimization of the modulation function (*a*) was performed by minimizing the dispersion of the Patterson function along u within the mask shown by the dotted line in (*d*) and (*e*).

However, we found that data collected from the two different lattices have identical modulation and therefore α is close to 1/2. Thus, as in the case of perfect twinning by merohedry, detwinning would not work for reflections with $q(h)$ close to 1. Fortunately, detwinning becomes feasible owing to the internal symmetry of a single OD layer. The Fourier transform amplitude of the layer's electron density has point-group symmetry that includes twinning operators. This means that overlapping reflections from the two lattices have very similar intensities. Moreover, the higher the overlap the closer the intensities are (indeed, R_{sym} with respect to the twinning operator for the subset of reflections with $h = 10n$ is 4.1% for observed and 11.9% for calculated intensities). Also, the less the overlap the less the contribution is from the alternative lattice and therefore less accurate estimates for intensities from the alternative lattice are required in (1). Thus, for the pairs of reflections related by (1), we assume that

$$I_1 = I_2 \quad (2)$$

and (1) can be rewritten as

$$I_T = [1 - \alpha + \alpha q(h)]I = q'(h)I. \quad (3)$$

This means that detwinning can be performed by pure demodulation, where the detwinned intensity is derived solely from the original intensity multiplied by a coefficient dependent on h . Similarly to $q(h)$ in (1), the coefficient $q'(h)$ in (3) can be modelled by a periodic function of h , where t approximately equals 1/10 and its exact value depends on the obliquity,

$$q'(h) = p_0 + p_1 \cos(2\pi th) + p_2 \cos(4\pi th) + \dots \quad (4)$$

Thus, the detwinning procedure must involve refinement of t , on which the overlap strongly depends. The coefficient p_0 is defined by the equation $q'(0) = 1$, which follows from $q(0) = 1$ and (3).

The demodulation was performed using a specially written Fortran program. Firstly, optimization of the parameters t, p_1, p_2, \dots (4) was performed by minimizing the dispersion of the Patterson function on the line $v = w = 0$ within a mask excluding an area around the origin (Figs. 4*d* and 4*e*). This was performed for zero to six harmonics in expansion (4). Secondly, the original data were demodulated by dividing the intensities by the corresponding value of $q'(h)$. Subsequently, restrained refinement using *REFMAC* was performed against each demodulated data set, starting each time from the same atomic model. The best $R = 0.162$ and $R_{\text{free}} = 0.225$ were obtained for the approximation (4) containing three harmonics. The corresponding modulation function $q'(h)$ is shown in Fig. 4(*a*). The refined value of t corresponds to an obliquity of 0.13°, which agrees with the values derived from the unit-cell parameters. The demodulated data give a relatively smooth plot of $\sum_k \sum_l I(h, k, l)$ against h (Fig. 4*c*) and the corresponding Patterson map contains no strong non-origin peaks (Fig. 4*e*).

OD structures with a large number of twinning interfaces are considered to be disordered OD structures (Dornberger-Schiff & Dunitz, 1965). They produce elongated reflections (stripes) on the diffraction images. The first case of a disordered macromolecular OD structure was reported by Bragg & Howells (1954), even before the first protein crystal structure was solved. Apparently, we have a case that is intermediate between a polysynthetic OD twin and a disordered OD structure, as stripes are present in some images (not shown). Nevertheless, the demodulation procedure remains applicable to such cases (Wang *et al.*, 2005).

Macromolecular crystals are characterized by a clearly defined hierarchy of building blocks and by the different strengths of inter-

actions between them. Because of this, protein crystals are frequently composed of symmetric layers with asymmetric interfaces between them (OD structures). In such cases, there is the potential for the formation of OD twins and allotwins (Nespolo *et al.*, 2004). An example of a macromolecular allotwin has been reported (Dauter *et al.*, 2005). The procedure described above is applicable to the majority of such cases where (i) the exact twinning operator can be identified based on the organization of the crystal and (ii) higher symmetry of OD layers can be further utilized to reduce detwinning to a simple demodulation, thereby avoiding the problem with singularity at $\alpha = 1/2$.

The Engineering and Physical Sciences Research Council, UK and TMO Renewables are acknowledged for PhD studentship funding to CAR. We thank Professor T. Oshima for providing the *S. tokodaii* genomic DNA and we thank Dr Roger Cripps for useful discussions. AAL was supported by an NIH grant (1ORI GM069758-03). The Synchrotron Radiation Source, Daresbury is acknowledged for provision of data-collection facilities on the NWSGC MAD10 beamline funded by BBSRC grants (719/B15474 and 719/REI20571) and an NWDA project award (N0002170).

References

- Allpress, J. D. & Gowland, P. C. (1998). *Biochem. Educ.* **26**, 267–276.
- Arai, R., Kukimoto-Niino, M., Kuroishi, C., Bessho, Y., Shirouzu, M. & Yokoyama, S. (2006). *Protein Sci.* **15**, 373–377.
- Bairoch, A. & Apweiler, R. (2000). *Nucleic Acids Res.* **28**, 45–48.
- Bragg, W. L. & Howells, E. R. (1954). *Acta Cryst.* **7**, 409–411.
- Cianci, M. *et al.* (2005). *J. Synchrotron Rad.* **12**, 455–466.
- Collaborative Computational Project, Number 4 (1994). *Acta Cryst.* **D50**, 760–763.
- Dauter, Z., Botos, I., LaRonde-LeBlanc, N. & Wlodawer, A. (2005). *Acta Cryst.* **D61**, 967–975.
- Dornberger-Schiff, K. (1956). *Acta Cryst.* **9**, 593–601.
- Dornberger-Schiff, K. & Dunitz, J. D. (1965). *Acta Cryst.* **19**, 471–472.
- Emsley, P. & Cowtan, K. (2004). *Acta Cryst.* **D60**, 2126–2132.
- Esnouf, R. M. (1999). *Acta Cryst.* **D55**, 938–940.
- Franken, S. M., Rozeboom, H. J., Kalk, K. H. & Dijkstra, B. W. (1991). *EMBO J.* **10**, 1297–1302.
- Gill, S. C. & von Hippel, P. H. (1989). *Anal. Biochem.* **182**, 319–326.
- Hill, K. E., Marchesi, J. R. & Weightman, A. J. (1999). *J. Bacteriol.* **181**, 2535–2547.
- Hisano, T., Hata, Y., Fujii, T., Liu, J. Q., Kurihara, T., Esaki, N. & Soda, K. (1996). *J. Biol. Chem.* **271**, 20322–20330.
- Holloway, P., Trevors, J. T. & Lee, H. (1998). *J. Microbiol. Methods*, **32**, 31–36.
- Kawarabayashi, Y. *et al.* (2001). *DNA Res.* **8**, 123–140.
- Koonin, E. V. & Tatusov, R. L. (1994). *J. Mol. Biol.* **244**, 125–132.
- Laemmli, U. K. (1970). *Nature (London)*, **227**, 680–685.
- Le Page, Y. (2002). *J. Appl. Cryst.* **35**, 175–181.
- Matthews, B. W. (1968). *J. Mol. Biol.* **33**, 491–497.
- Murshudov, G. N., Vagin, A. A. & Dodson, E. J. (1997). *Acta Cryst.* **D53**, 240–255.
- Nespolo, M., Ferraris, G., Durovic, S. & Takeuchi, Y. (2004). *Z. Kristallogr.* **219**, 773–778.
- Otwinowski, Z. & Minor, W. (1997). *Methods Enzymol.* **267**, 21839–21843.
- Perrakis, A., Morris, R. M. & Lamzin, V. S. (1999). *Nature Struct. Biol.* **6**, 458–463.
- Slater, J. H. (1982). *S. Afr. J. Sci.* **78**, 101–104.
- Slater, J. H., Bull, A. T. & Hardman, D. J. (1997). *Adv. Microb. Physiol.* **38**, 133–176.
- Vagin, A. A. & Teplyakov, A. (1997). *J. Appl. Cryst.* **30**, 1022–1025.
- Wang, J., Kamtekar, S., Berman, A. J. & Steitz, T. A. (2005). *Acta Cryst.* **D61**, 67–74.
- Warburg, O. & Christian, W. (1941). *Biochem. Z.* **310**, 384–421.
- Woese, C. R., Kandler, O. & Wheelis, M. L. (1990). *Proc. Natl Acad. Sci. USA*, **87**, 576–579.